IEEE Access
Multidisciplinary | Rapid Review | Open Access Journal

Received 22 August 2023, accepted 16 September 2023, date of publication 22 September 2023, date of current version 4 October 2023.

Digital Object Identifier 10.1109/ACCESS.2023.3318171

RESEARCH ARTICLE

A Novel Approach to Monitor Head Movement Inside an MR Scanner Using Voltages Induced in Coils by Time-Varying Gradients

ENAMUL H. BHUIYAN[1,2], MUHAMMAD E. H. CHOWDHURY[3], (Senior Member, IEEE), AND PAUL M. GLOVER[2]

[1]Center for Magnetic Resonance Research, University of Illinois at Chicago, Chicago, IL 60612, USA
[2]Sir Peter Mansfield Imaging Centre, School of Physics and Astronomy, University of Nottingham, NG7 2RD Nottingham, U.K.
[3]Department of Electrical Engineering, Qatar University, Doha, Qatar

Corresponding authors: Enamul H. Bhuiyan (hoque.phy@gmail.com) and Muhammad E. H. Chowdhury (mchowdhury@qu.edu.qa)

This work was supported by Qatar National Library (QNL).

This work involved human subjects in its research. Approval of all ethical and experimental procedures and protocols was granted by the Sir Peter Mansfield Imaging Centre (SPMIC), University of Nottingham, Nottingham, U.K.

ABSTRACT To determine head pose within an MR scanner using measurements of gradient-induced voltage from a multiple coil. A practical implementation of this approach would involve measuring the position-sensitive voltages induced by the imaging gradients rather than additional gradient pulses. This would speed up the model formation phase and increase the temporal resolution of position monitoring. We propose a novel method to measure the gradient-induced voltages in a set of five coils to estimate the position and orientations (POS) into MR scanner. A training set of measurements was first made and then Principal Component Analysis (PCA) was applied to the POS data estimated by using Statistical Parametric Mapping (SPM8), and the principal components were collected into a design matrix. Experimental data were collected and then the coefficients derived from the training set were used to estimate the POS changes and the results compared to movement parameters found using image co-registration. The changes in POS estimated from SPM8 co-registration and from the measured voltages for the phantom and the subject. The differences in the positions were estimated by using SPM8 and the model relating the change in induced voltages to position. The range and root-mean-square (RMS) amplitude of these differences for the phantom/subject data. The results suggest that it is possible to estimate the position and orientation with 0.22mm and 0.24° root-mean-square error using this set-up. The new approach could be used for prospective or retrospective motion correction.

INDEX TERMS Head motion, gradient pre-pulse, coils array, time-varying gradient, multivariate analysis, general linear model, motion tracking.

I. INTRODUCTION

Despite MRI advancements, patient movements during scans remain a challenge. About one in five MRI scans needs repeating due to motion, increasing healthcare costs by nearly $1 billion [1] [2]. The issue is common in non-compliant patient groups: children, infants [3], [4], trauma/stroke patients [5], those with anxiety, pain, or movement disorders like Parkinson's [6], and patients with Alzheimer's [7], Huntington's [8], and multiple sclerosis [9]. Using motion correction techniques could cut costs, making MRI more accessible, and benefiting more people.

In functional MRI (fMRI) time series, movement between consecutive acquisitions of the same slice leads to image mis-registration which can produce spurious activation in fMRI data. In anatomical MRI, movement between

The associate editor coordinating the review of this manuscript and approving it for publication was Jinhua Sheng.

acquisitions of different data segments in k-space (the Fourier domain) generates image artefacts [10]. If movement information is recorded and processed during the image acquisition it is possible to adjust the image acquisition geometry [10] in ''real time'' so that the artefacts are eliminated.

Several techniques [11], [12], [13], [14], [15] have been developed to monitor head motion during MRI scans, including optical tracking, small NMR coils, real-time intra-volume motion correction with active markers [16], head position prediction during rapid subject motion [17], real-time slice-by-slice motion correction for fMRI in freely moving subjects [18], and combining prospective motion and distortion correction for EPI [19].

Optical methods include laser systems [20], [21], optical fibers [22], and camera systems. Optical tracking work began with the use of out of-bore camera systems by Zaitsev et al. [23], but it has now moved to in-bore camera systems. Methods successfully used for motion correction include out-of-bore stereo camera systems [18], [23], out-of-bore single camera systems [24], in-bore single camera systems [11], [25], and in-bore systems with multiple cameras [26], [27]. Schulz et al. [28] used a novel home-built optical embedded tracking system for motion-corrected magnetic resonance imaging at 7T. On the other hand, Formana et al. [29] used a novel self-encoded marker to overcome the limited tracking range of the head position inside the camera's narrow field of view (FOV). Almost all optical systems require a marker, which must be rigidly attached to the head. Researchers are now trying to develop markerless optical tracking [30], [31] systems, since this will form an ideal technique from a patient handling perspective.

Field detection methods have a long history in MRI. Although Dumoulin et al. [32] pioneered developments in this area; this method was first introduced by Ackerman et al. [33]. A study of slice-by-slice prospective motion correction using such a system was published by Derbyshire et al. [34]. Recent implementations, such as that of Ooi et al. [35], [36] characterize the RF coil/material combination as ''active markers.'' Active markers have been used for prospective motion correction in structural brain scans [35] and in echo-planar imaging (EPI) [36]. A similar technique recently applied to measure gradient waveforms by Barmet et al. [37], [38], who decouple tracking from MR imaging by using RF-shielded probes and separate transmit or receive chains. Micro radio frequency coil ''active markers'' have also been used by [38] for real-time slice-by-slice prospective correction. Recently Melvyn et al. [39] used inductively coupled wireless radio frequency (RF) coils (wireless markers) for position tracking. Lei et al. [40] used an array of intra-cavity imaging coils for prospective motion correction. In Refs. [35], [36], marker fixation was achieved by attaching the coils to a headband worn by the subject has a slight disadvantage over optical methods here, as the active markers (and hence the subject) are connected to the scanner by wires, which makes patient handling more difficult and could perhaps increase the patient's anxiety levels.

Navigator methods are a more traditional way of obtaining object position information during MRI. Recent examples include navigators operating in k-space, such as cloverleaf navigators [41], orbital navigators [42]. Cloverleaf navigators [41] can be used to measure and correct rigid body motion and associated first-order shim changes in real time. Spherical navigator echoes [43] use a 3D spherical navigator (SNAV) echo technique that can measure rigid body motion in all six degrees of freedom simultaneously by sampling a spherical shell in k-space. None of the existing methods is perfect, and the best choice of method will depend on the relative importance of the three criteria: high accuracy and precision, no patient interaction, and sequence independence [17].

Besides these methods, there are image-based tracking methods, such as PROMO [44] or EPI navigators [45], [46], Sparsity and Kalman Filtering [47] and PROPELLER [48]. These require longer acquisitions than k-space navigators but allow the user to define the region of interest for motion quantification, thus avoiding non-rigid regions (e.g., the neck). Alternatively, it is possible to detect, but not quantify, motion by comparing the relative intensity of a free induction decay signal between multiple receive coils [14].

Although difierent techniques have been developed for preventing motion artefacts, in the case of clinical scanning none of the methods work adequately at present. All these methods have advantages and disadvantages. Optical tracking is accurate and fast, but costly and requires line of sight access to the head, whereas the navigator methods are fast, but require imaging sequence modification. On the other hand, image-based tracking is accurate, but slow. Some of the methods require additional hardware. The challenge is to track involuntary movements of the patient's head in an MR scanner. In this study, we aim to track involuntary head movement by measuring the voltages induced by gradient switching in a set of coils attached to the head. By considering the human head as a rigid body this will allow us to apply prospective motion correction in MRI.

This study proposes using a set of inductive coils woven into a cap placed on the scalp to measure motion. This will be accomplished by monitoring the voltages induced in the coils by the time-varying magnetic field gradients applied in the MRI sequence and relating the changes in the induced voltages to changes in head position and orientation. The voltages can be recorded by connecting an EEG amplifier to the coils.

Previous work has suggested that head movement can be monitored by using measurements of the change with respect to position of the voltages induced in a set of coils by time-varying magnetic field gradients [49], [50], [51], [52]. Particularly, in high field MRI the image resolution can be a less than a millimeter and even such a very small movement can cause substantial artefacts [28]. In recent years many motion correction techniques have been suggested, but none

of the devices or methods proposed so far produces a workable solution for clinical use. The use of gradient-induced voltages in coils attached to the subject has potential advantages over other motion monitoring techniques [10], [35], [50], as it does not require line-of-sight access to the subject or significant modification of the imaging sequence.

This study firstly focuses on optimization of gradient pre-pulses for position monitoring. A drift is observed in the voltages recorded from the EPI pre-pulses using the coils. It is found to depend mainly on the time delay between pulses. This study also checked the TR dependency of the voltages due to EPI pre-pulses. This was done by measuring the voltage induced in the coils by three gradient pre-pulses successively applied on the RL, AP and FH axes with varying delays between the pulses.

Secondly, this study evaluates the use of principal component analysis (PCA) for simplifying the process of fitting the measured voltages to the head movement. PCA is probably the most popular multivariate statistical technique, which uses sophisticated underlying mathematical principles and is used in almost all scientific disciplines. It analyses a data table in which observations are described by several inter-correlated, dependent variables. Its goal is to extract important information from the data, to represent it using a new set of orthogonal variables, called the principal components. In general terms, principal component analysis uses a vector space transform to reduce the dimensionality of large data sets. Using mathematical projection, the original data set, which may have involved many variables, can often be interpreted using just a few variables (the principal components) [53], [54].

The approach described here, which could be used for prospective or retrospective motion correction, involves characterizing the relationship between head pose and the induced voltages in an initial set of imaging experiments, and subsequently using this relationship to calculate changes in head position and orientation from the measured voltages. This approach was tested by attaching five coils to a structured, spherical agar phantom, which was then placed in a gimbal system that allowed controlled rotation about the right-left (RL = x) and foot-head (FH = z) directions, as well as translation in the z-direction. The approach was then evaluated in experiments on a human subject, in which the coils were attached to the head.

The background theory and the feasibility [55] of this experimental work were thoroughly studied using a generalized linear model by Bhuiyan et al. Roth et al. [56] disclosed a tracking system based on the gradient fields of magnetic resonance imaging (MRI) scanners by using custom sequence without any change of the scanner's hardware or mode of operation. Recently, Frost et al. [57] explored high-frequency movement correction during imaging echo trains to combine markerless head motion with prospectively corrected neuroanatomical MRI sequence. Lauesten et al. [58] used electroencephalography (EEG) hardware for recording signals induced by native imaging gradients for tracking head movement and estimated motion from recordings of gradient switching. Afacan O. et al. [59] modified MPRAGE sequence to measure motion using the EM tracking system once per repetition time. There are some other techniques used NMR probes [60], sensor [61] and stripe structure light [62].

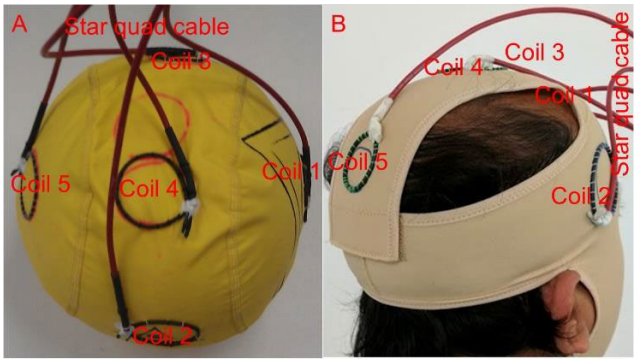

FIGURE 1. Set of five coils attached to (A) a spherical agar phantom (all coils had ∼ 4 cm diameter and 2 turns) and (B) a healthy human subject (Coils 1-3 coils had ∼4 cm diameter and 2 turns, while Coils 4 and 5 had ∼ 3 cm diameter and 3 turns). Coils were connected to the ExG bipolar amplifier (Brain Products GmbH) using star quad cable (Van Damme) minimizing the induced voltage contribution from the cables. Coils are connected to the ExG amplifier through 100kΩ resistors.

II. METERIALS AND METHODS

A spherical head phantom, a gimbal to hold the phantom and the coils (2-turns in each) mounted onto an EEG-like cap were used to perform the experiments. The gimbal is clamped on to the patient's bed and the coils are mounted onto a cap fitted on the spherical head phantom, as shown in Figure 1(A). For the experiments on the human subject the coils were mounted onto a thin face mask, as shown in Figure 1(B).

In both cases, the coils are made up of copper wire of 0.224mm diameter coated with heat shrink to avoid deformation. The coils are connected to 5-channels of a 16-channel bipolar amplifier using star quad cable (Van Damme). The use of star quad cable reduces the magnitude of any voltages induced in the cables by gradient switching or movement in the B0 -field. There are four cores of wires very tightly twisted with each other and rotate over a relatively short length. This arrangement ensures a magnetically coaxial structure and offers significantly enhanced rejection of electromagnetic interference relative to standard two core mic cables. The body RF coil was used for experiments on the phantom, while a 32-channel head Rx coil was used for experiments on the human subject. The coils were attached to the cap/mask by sewing using thread and needle. The coil voltages were recorded using a BrainAmp MR plus EEG amplifier and Brain Vision Recorder software (Brain Products, Gilching, Germany). The EEG system allowed recording of signals in the frequency range 0.016–250 Hz with a sampling rate of 5 kHz. The MR scanning and EEG sampling were synchronized by driving the EEG amplifier clock using a 5 kHz signal derived from a 10 MHz reference signal from the MR scanner [63].

For the initial experiments, we used an EPI sequence which included three additional gradient pulses successively applied along the right-left (RL), anterior-posterior (AP) and foot-head (FH) directions, applied in the quiet periods between slice acquisitions. Each pulse ramped-up/down over 5ms at 4T/m-s inducing voltages of several hundreds of μV in the coils, as shown in Figure 2.

This sequence was run with a long TR (48s) to allow large temporal separation of pre-pulses thus limiting any effect of vibration. In later experiments, we changed the sequence so that a single gradient pre-pulse was applied with each EPI slice acquisition for the gradient direction cycling RL$\rightarrow$AP$\rightarrow$FH across successive volume or slice acquisitions. This allowed us to reduce the TR to a more realistic value of 2s.

The voltage changes in the coils and their linear fittings in case of translation along the z-axis for the x-gradient pre-pulse is shown in Figure 3. Slopes are obtained from linear fits. Again, the change in induced voltage in the coils due to sequential rotation about the z-axis for a range of -10 to $+10^\circ$ is linear with respect to rotational angle. Linearity does not break for a wide range of rotations about the x- and z-axis. On the other hand, linearity persists for any range of translation along the z-axis. Figure 3 shows the voltage change in the coils and their linear fits. It is interesting that linearity persists for a wide range of rotations ranging from -10 to $+10^\circ$.

From image realignment using SPM8, the movement parameters are obtained for three movements (head-nod, headshake, and z-translation). The change in induced voltage in the coils versus movement parameters obtained from image realignment is plotted and the corresponding slopes are determined from linear fittings of the voltage. By using these slopes, a 9×3 matrix is formed which is known as A. A system of linear equations is formed in the matrix form as $\delta V = A\delta r$, where $\delta r = [\delta z, \delta\theta, \delta\psi]$ and $\delta V = [\delta Vz, \delta V\theta, \delta V\psi]$.

In the case of EPI pre-pulses applied in conjunction with a long TR period (TR = 48s), the position (x, y and z) and orientation (θ, φ and ψ) of the phantom was also measured by using SPM8 to co-register gradient echo (GE) images [$(1.5 \times 1.5 \times 1.5)$ mm^3 resolution; FOV = $(240 \times 240 \times 96)$ mm^3; 144s acquisition time for 2 dynamics]. For the human subject, the poses were also measured by using GE-EPI images of $(3.0 \times 3.0 \times 3.0)$ mm^3 resolution; FOV = $(240 \times 240 \times 96)$ mm^3; 624s acquisition time for 12 dynamics.

For the repetition of pre-pulses in each dynamic and with a short TR period (TR = 2s), the positions (x, y, and z) and orientations (θ, φ, and ψ) of the phantom were also measured by co-registering images acquired during the experiments using the Statistical Parametric Mapping toolbox (SPM8). 3D gradient echo images with resolution $(3.0 \times 3.0 \times 3.0)$ mm^3 resolution; FOV = $(240 \times 240 \times 60)$ mm^3; scan duration 366 s were used for the phantom, whereas the EPI images of $(3.0 \times 3.0 \times 3.0)$ mm^3; FOV = $(240 \times 240 \times 78)$ mm^3; 26 slices in each dynamic were used for the subject.

Before performing the experiment on phantom or on human subjects, the volunteers were given instructions regarding the nature of the movements during the model formation period (cued movement) and the experimental period (random movement).

A. MULTIVARIATE ANALYSIS

Multivariate analysis is used here to avoid the risk of over fitting and reduced the dimensionality of the movement parameters obtained from image co-registration by using SPM8. For this purpose, a training set of measurements was first made while the phantom/head was translated along the z-axis and then rotated about the x- and z-axes. Principal Component Analysis was applied to the position data estimated using SPM8 to identify the combination of parameter changes that best characterized the movements, and three (three movements are dominating: axial translation, headshake, and head-nod) principal components were then collected together into a design matrix along with a baseline term. A general linear model (GLM) is used to form the design matrix. The design matrix was fitted to the measured voltages (voltages were measured from 5 coils for three gradient pre-pulses, yielding 15 independent voltage measurements) using a pseudo-inverse to determine the coefficients relating the co-ordinate changes and induced voltages. Experimental data were then collected while the subject/phantom underwent random changes in position. The coefficients derived from the training set were used to estimate the position changes and the results compared to movement parameters found using image co-registration. The whole process is summarized in the flow diagram shown in Figure 4.

III. RESULTS

In initial experiments, we found that vibration produced by early pre-pulses affects the recording of voltages from later pre-pulses because any coil rotation in the strong B_0-field produces additional induced voltages. By varying the time delay between pulses as well as the TR one can optimize the pre-pulses.

Time delays between the pre-pulses of 100ms, 200ms, 400 ms and 500ms were tested. It is tested for TR values of 7.5s and 10s by taking 10 slices per TR period. From analyzing the voltages induced by the pre-pulses one can conclude that the drift observed in the voltages due to the pre-pulses mainly depends on the time delays between pre-pulses rather than on the TR. One can reduce the drift in the expected recorded voltage pulse shapes by tuning the time delays between pulses. In this work, we found that an inter-pulse delay of 400ms gave acceptable results.

A. MODEL FORMATION

Here, twelve measurements were made with the phantom first rotated about the x-axis and then about the z-axis, before being translated to different z-positions. Principal Component Analysis was applied to these data to identify

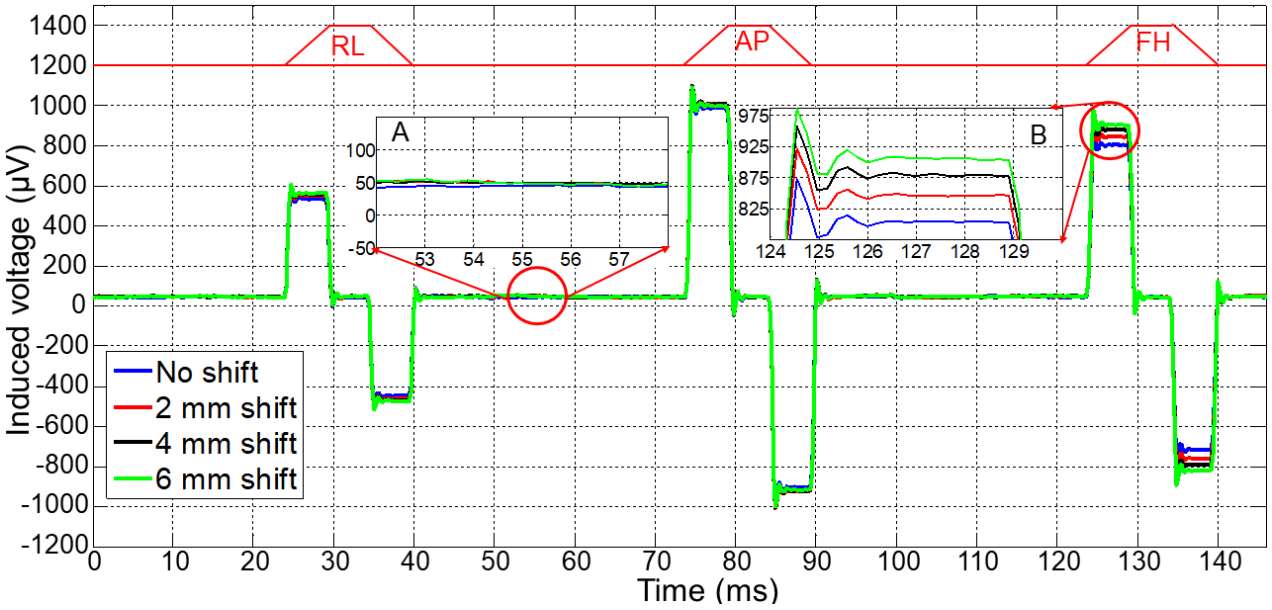

FIGURE 2. Voltages induced in a single coil mounted on a phantom by application of a sequence of three trapezoidal gradient pulses (5 ms ramp- up/down at 4 /m-s) successively applied along the RL, AP and FH directions. The position of the phantom was shifted away from iso-centre in the FH direction in steps of 2 mm causing the amplitude of the induced voltages to change. The results are shown for 4 different positions of the phantom. Inset A shows no appreciable change in the baseline recording with respect to successive movements, whereas inset B shows a linear increase in the voltage induced by the FH trapezoidal pulse as the FH shift increases.

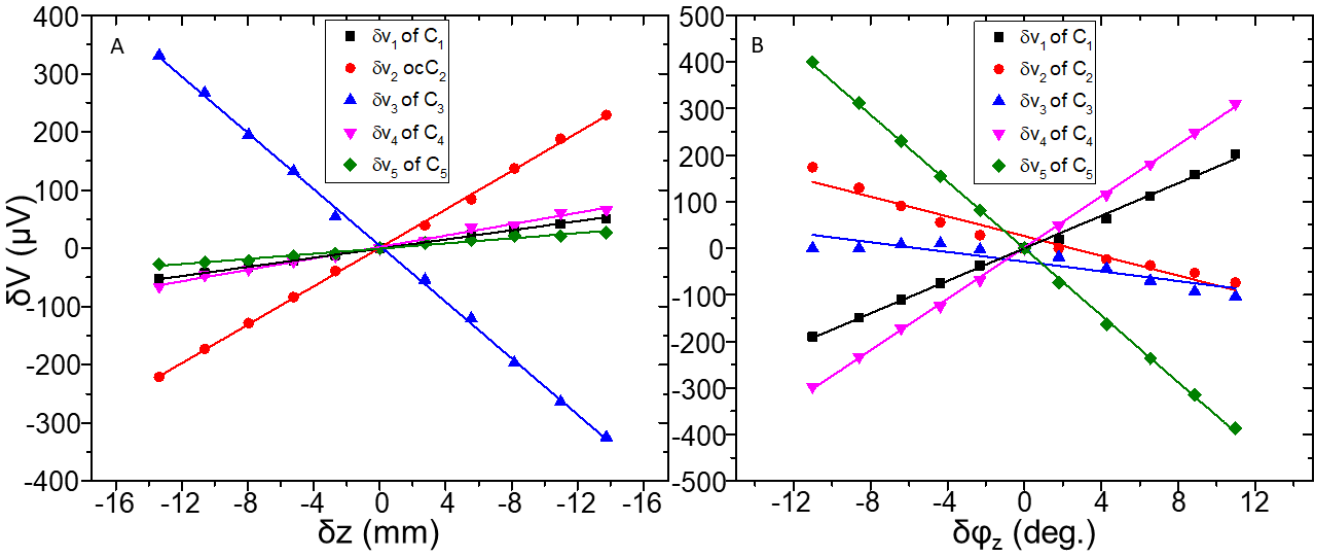

FIGURE 3. Experimental data indicates induced voltage change in the coils and their linear fittings. (A) The change in induced voltage in the coils due to x-translation during the execution of x-gradient and their linear fittings. (B) The change in induced voltage in the coils due to z-rotation during the execution of x-gradient and their linear fittings.

the combination of parameter changes that best characterized the movements, and three principal components were then collected into a general linear model that was fitted to the measured voltage changes. Three measurements were subsequently left out of the model formation phase and the resulting model used to identify the phantom position from the voltage measurements. The results were then compared to parameters identified using the SPM8 registration.

In Figure 5(A), a graphical representation illustrates a dataset composed of 12 data points, with each category of movement parameters (head-nod, headshake, and axial-translation) contributing 4 data points. The focus is on three principal component analysis (PCA) components. Notably, three points (specifically the 3rd, 7th, and 11th) have been excluded from this presentation.

In Figure 5(B), the emphasis shifts to showcasing the disparities or errors that arise when comparing parameters estimated using coils versus those obtained using SPM8. This figure captures the intricacies of the differences between the two methodologies.

Figure 5 shows important observation. The initial quartet of data points in this figure represents the influence of

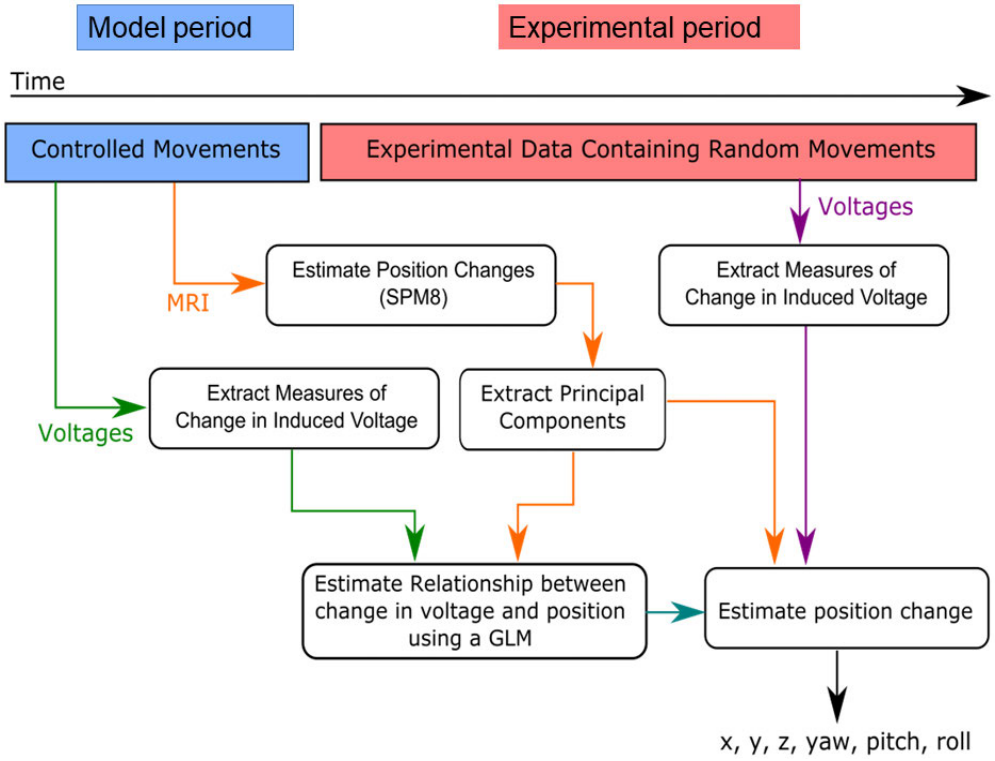

FIGURE 4. Flow diagram for multivariate analysis.

x-rotation, while the subsequent set of four points delves into the impact of z-rotation. The final set of points within this visualization pertains to the z-translation effects observed in the context of the spherical head phantom. This visualization allows for a comprehensive understanding of the dynamics and discrepancies between the methods employed, offering insights into the study's findings.

B. RECORDINGS FOR LONG TR PERIOD

1) PHANTOM

The construction of the model involves the incorporation of data collected at twelve distinct time-points throughout the model formation phase, during which controlled movements are executed. Subsequently, during the experimental phase, a total of fourteen data points is captured, corresponding to fourteen random movements of the phantom. The data from the model formation phase are meticulously analyzed to enable the prediction of the positions of the fourteen points recorded during the experimental phase. The outcomes of this prediction process are depicted in Figure 6(A), which offers a visual representation of the achieved results. Additionally, Figure 6(B) provides a comprehensive visualization of the errors associated with the estimated parameters, offering valuable insights into the accuracy and robustness of the model's predictions.

2) SUBJECT

In this particular scenario, the model is developed with a comprehensive structure comprising seven distinct points. Among these, one point represents the initial position, while the remaining six correspond to controlled movements encompassing axial-translation, headshake, and head-nod. Specifically, there are two points allocated to each of these controlled movements during the model formation phase. Subsequently, during the experimental phase, five points are sampled to correspond to five random movements executed by the subject's head.

In a manner analogous to the approach used during the model formation phase, a comparable methodology is employed to predict the five points associated with the experimental phase, but exclusively for the three PCA directions. This predictive process is visually presented in Figure 7(A). Conversely, Figure 7(B) visually illustrates the discrepancies or errors observed in the estimated parameters.

Notably, when focusing on the model formation phase (depicted solely in Figure 5), the model demonstrates exceptional precision in fitting the excluded points. Furthermore, the differences noted between the estimated parameters are exceptionally small, with translation discrepancies not exceeding 0.4 mm and rotational discrepancies remaining under 0.3 degrees. This model's remarkable capabilities are further highlighted by its successful utilization in accurately estimating both the position and orientation of an object within the MRI scanner. This estimation is achieved with a high degree of accuracy, ensuring that the achieved precision remains within 0.7 mm and 0.3 degrees.

To summarize, the findings indicate a robust agreement between the estimated parameters derived from SPM8 and

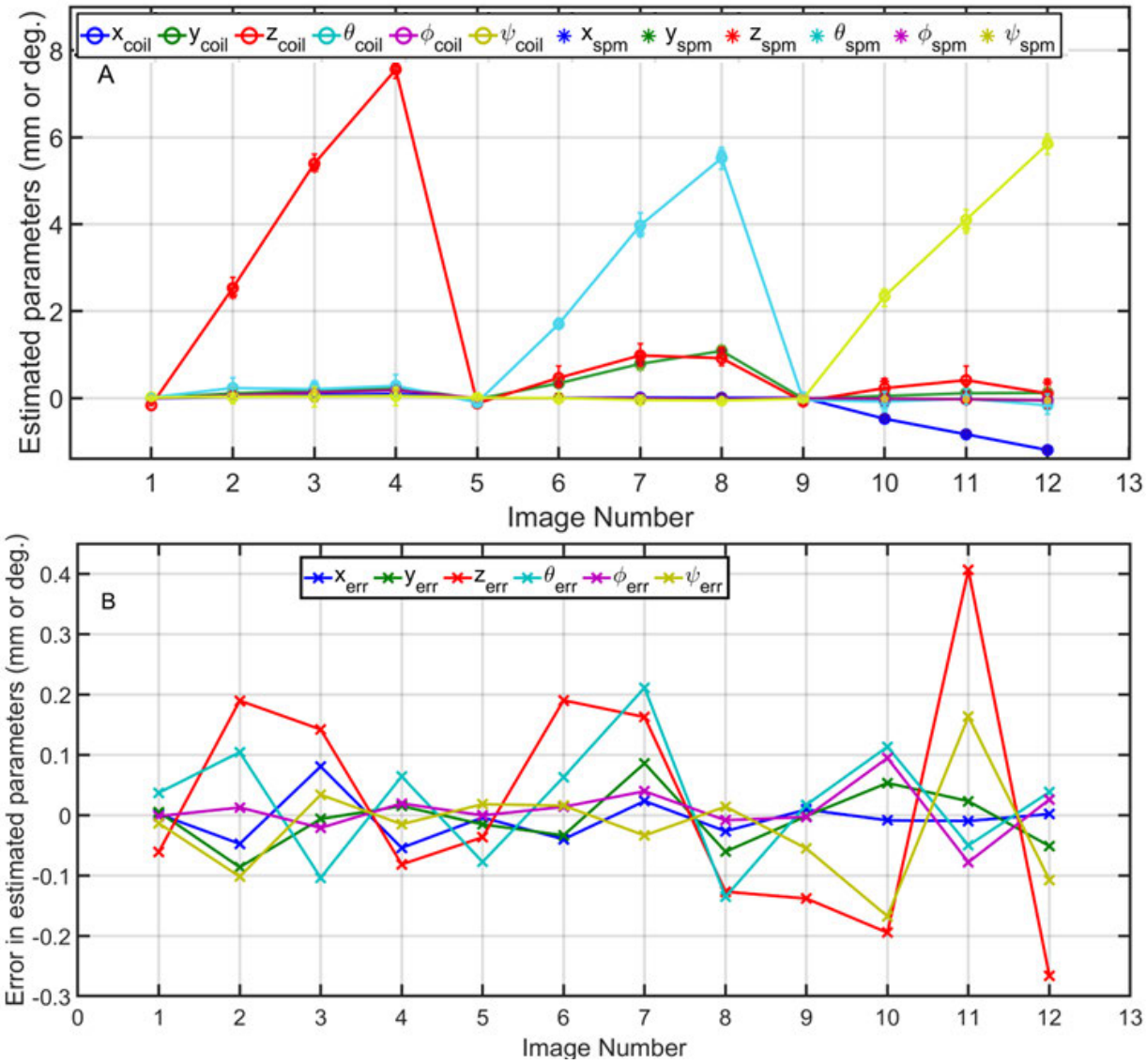

FIGURE 5. Data represents the movements parameters estimated by measuring the changes in induced voltage in the coils by time varying gradient magnetic field. Parameters estimated by using the induced voltages (°) and SPM8 (∗). 12 data points are estimated for 4 consecutive movements and excluding 3 data points, (3rd, 7th and 11th) one from each type of movement, end up with 9 data points that are used to form the model, which is then applied to find position for the 12 data points are shown in (A) for the phantom. The difference (×) between the parameters estimated with the coils (°) and using SPM8 (∗) is shown in (B) for the phantom.

those obtained from induced voltages, highlighting a strong linear relationship between the amplitudes of induced voltages and their respective positions and orientations. During the model formation phase, the model's predictive capabilities are demonstrated by accurately forecasting object positions at excluded time-points. Notably, the disparities in estimated parameters remain minimal, with translation discrepancies not exceeding 0.4mm and rotational variations not exceeding 0.3 degrees. This model is effectively harnessed to precisely determine the position and orientation of an object within the MRI scanner, achieving an impressive accuracy of 0.7mm and 0.7 degrees.

The standard errors in estimated positions for both the phantom and the human subject are consolidated in Table 1. The data underscores the remarkable precision of this approach, with errors in translation for the phantom being within 0.66mm and rotational errors within 0.67 degrees. Similarly, for the human subject, translation errors remain under 0.99mm, and rotational errors are contained within 0.89 degrees. Specifically, the results from the phantom demonstrate the potential to achieve estimates of position and orientation with a root mean square (RMS) error of less than 0.21mm and 0.23 degrees. Likewise, for the human subject, the model showcases its capacity to provide estimates of position and orientation with an RMS error of less than 0.22mm and 0.24 degrees, even for head movements within the range of ±4mm/degrees (as detailed in Table 1). These outcomes underscore the effectiveness of the proposed approach in accurately determining object positions and orientations within the MRI environment, fostering

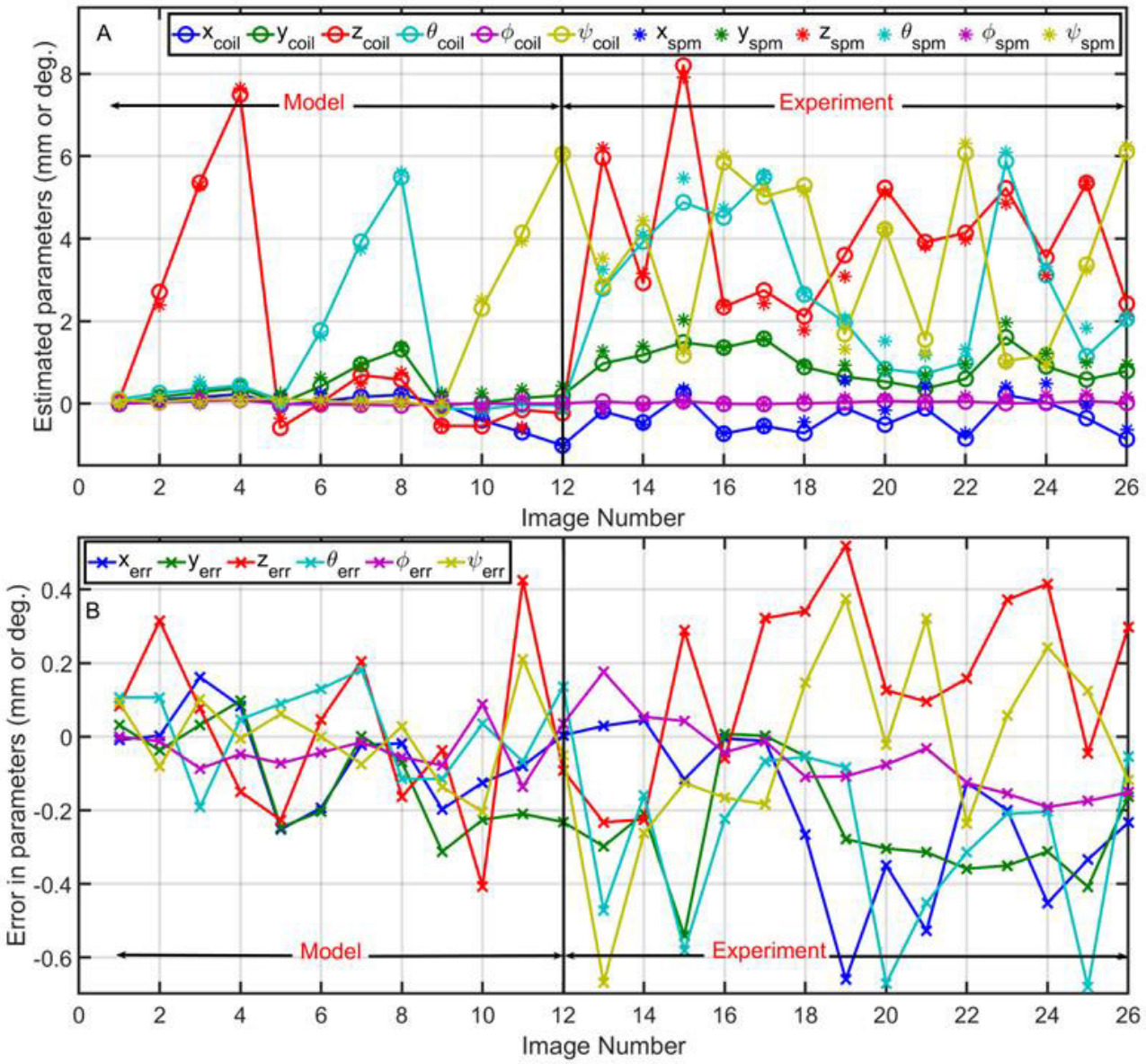

FIGURE 6. Change in position and orientation for phantom (A). Data collection was split into a model-forming period during which positions were successively adjusted along/about a particular axis and an experimental period during which positions were randomly varied. The changes in voltages with position were characterized using data from the model-forming period. This characterization was used to estimate the position change from the voltage recordings collected during the whole experiment. The differences (×) between the position estimated with the coils (°) and using SPM8 (∗) is shown in (B) for the phantom.

confidence in its applicability for diverse experimental scenarios.

C. RECORDINGS FOR SHORT TR PERIOD

For these experiments, we used an EPI sequence which included one gradient pre-pulse which was cycled across the image volume or slice acquisition along the right-left (RL), anterior-posterior (AP) and foot-head (FH) directions. Each pulse ramped-up/down over 2ms at 4Tm^{-1} s^{-1} inducing voltages of several $100\mu\text{V}$ in the coils.

The positions (x, y, and z) and orientations (θ, φ, and ψ) of the head/phantom were estimated by measuring the induced voltages in the coils and measured by co-registering images acquired during the experiments using the Statistical Parametric Mapping toolbox (SPM8). The EPI data ($3 \times 3 \times 3$) mm^3 resolution, FOV = ($240 \times 240 \times 60$) mm^3 for the phantom and FOV = ($240 \times 240 \times 76$) mm^3 for the subject was used for image registration in this case.

Voltage measurements were made due to cued axial-translation, headshake, and head-nod and for a set of random movements. Data recorded during movement instances were excluded due to artefacts caused by induced voltage in the coils resulting from rotation in the strong B0 field. 2 axial-translations; 2 head-shake rotations and 2 head-nod rotations were used to form a model and then 5 random movements were made, and the position changes due to the random movements were predicted from the model.

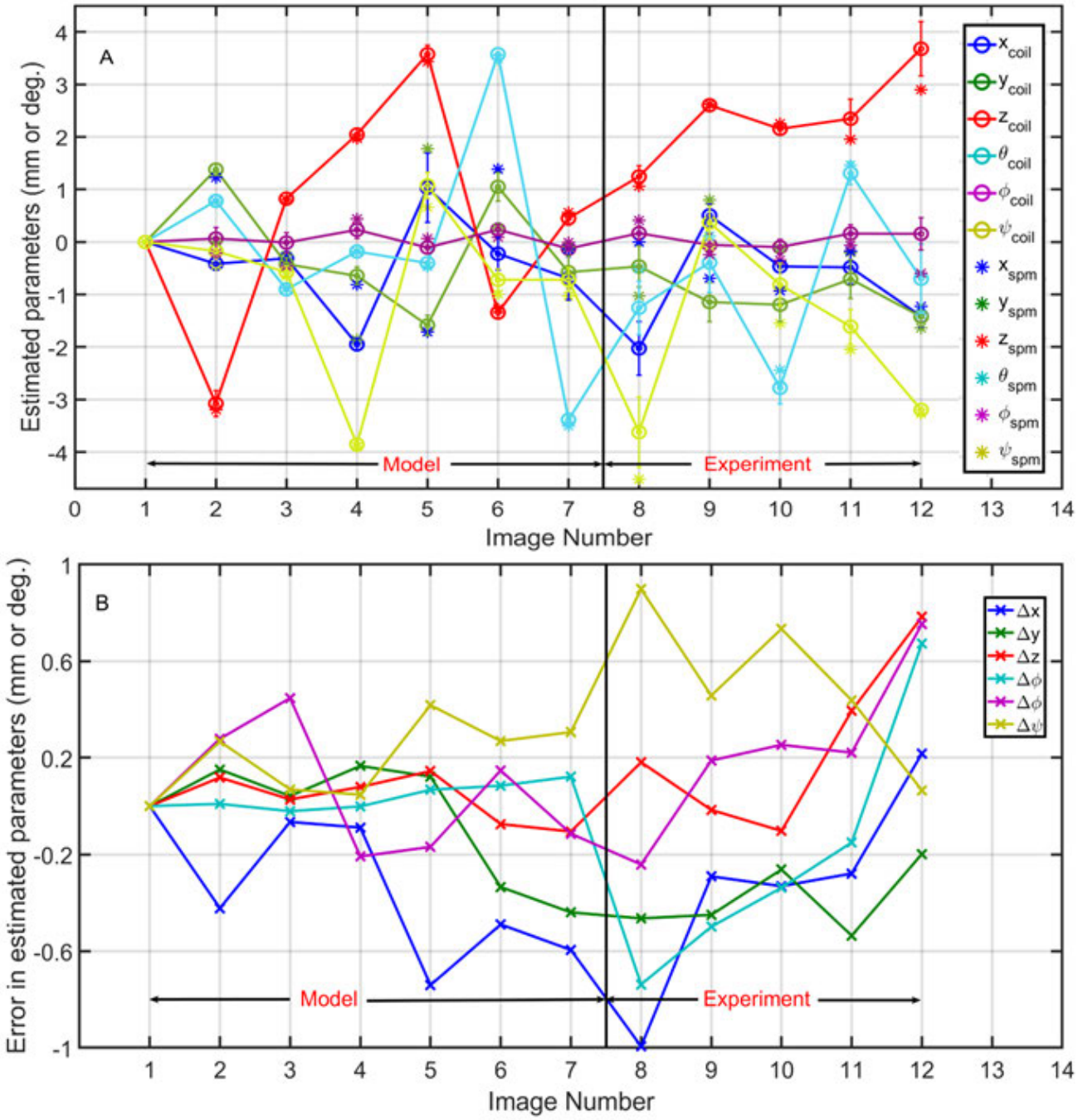

FIGURE 7. Change in position and orientation for subject (A). Data collection was split into a model-forming period during which positions were successively adjusted along/about a particular axis and an experimental period during which positions were randomly varied. The changes in voltages with position were characterized using data from the model-forming period. This characterization was used to estimate the position change from the voltage recordings collected during the whole experiment. The differences (×) between the position estimated with the coils (°) and using SPM8 (∗) is shown in (B) for the subject.

Phantom: Single Pre-pulses per Slice Acquisition Cycled over Volume Acquisition

The recordings were obtained using imaging parameters including a repetition time (TR) of 2000 ms, consisting of 180 volumes and 20 slices in each dynamic acquisition. Among these volumes, those corresponding to instances of movement were isolated from the acquisition. Averaging was performed across three consecutive RL (Right to Left), AP (Anterior to Posterior), and FH (Foot to Head) gradients. This preprocessing resulted in a refined dataset of 49 volumes, a reduction from the initial 60 volumes, as illustrated in Figure 8. Notably, data points were specifically selected to account for axial translation, head shake, head nod, as well as five distinct random movements.

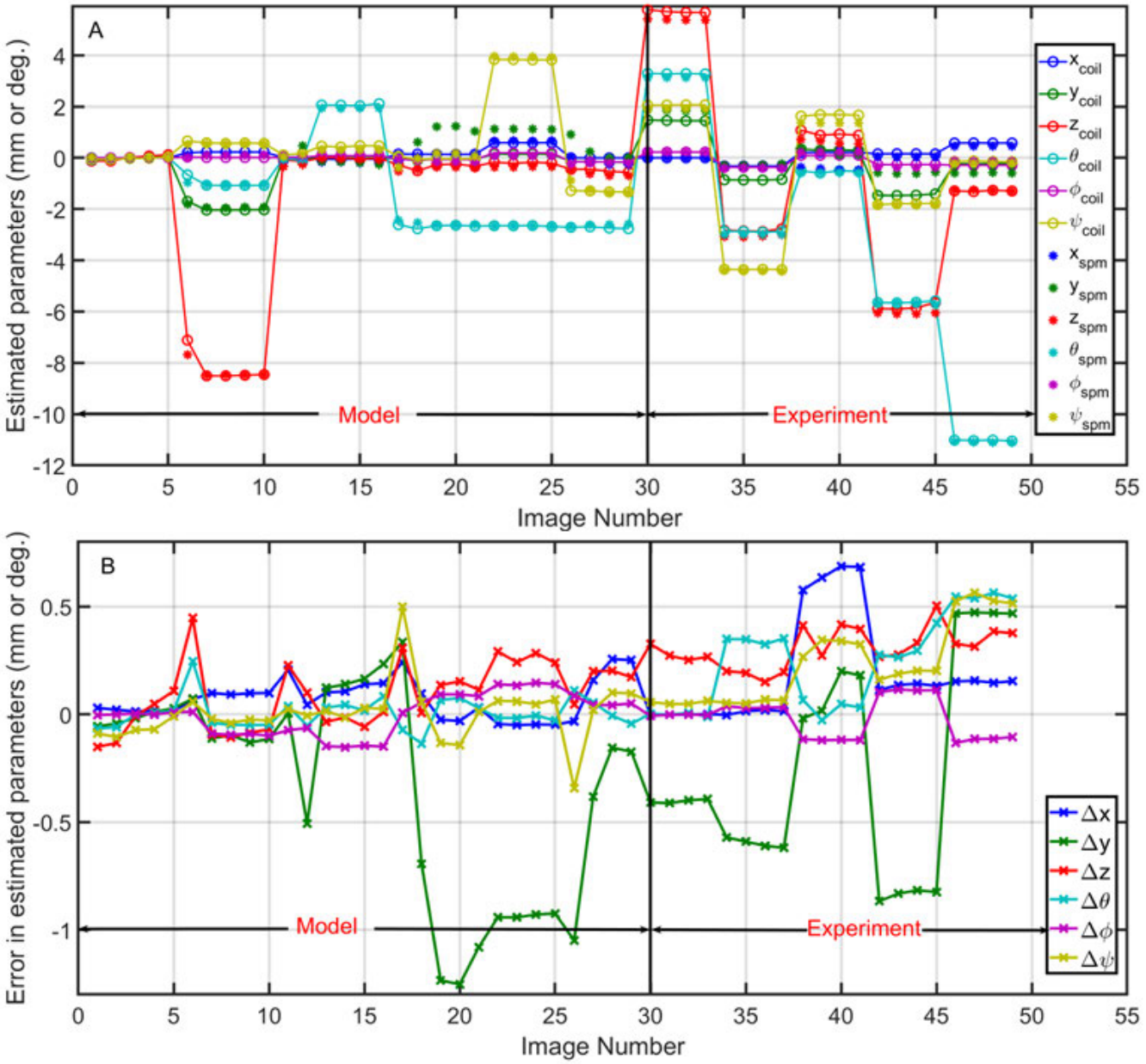

FIGURE 8. Measurements were made with short TR (TR = 2s) during scanning of the spherical agar phantom with a single pre-pulse applied per slice acquisition and the direction of the pre-pulse gradient cycled across volume acquisition. Changes in position and orientation for phantom (A). Data collection was split into a model-forming period during which positions were successively adjusted along/about a particular axis and an experimental period during which positions were randomly varied. The changes in voltages with position were characterized using data from the model-forming period. This characterization was used to estimate the position change from the voltage recordings collected during the whole experiment. The differences (×) between the position estimated with the coils (°) and using SPM8 (∗) is shown in (B) for the phantom.

In Figure 8, a set of 30 data points was employed to establish the model. This model was subsequently utilized to predict positions for all data points. The outcomes revealed that the maximum translation observed was approximately 9 mm, whereas the maximum rotation reached around 12 degrees. Importantly, the analysis indicated a high level of accuracy in the results. The maximum error in translation was found to be less than 0.4 mm, while in the case of rotation, it was less than 1.3 degrees. These findings underscore the effectiveness of the proposed methodology in accurately assessing movements and rotations in the acquired data.

Subject: Single Pre-pulses per Slice Acquisition Cycled over Volume Acquisition

The gradients are applied in a cyclical manner, with a volume-by-volume approach, where the repetition time (TR) is set at 2000ms, and 26 slices are acquired within each of the 180 volumes. Subsequently, 11 volumes containing motion artifacts are excluded from the acquired data, and the remaining data points are averaged for consecutive RL (right-to-left), AP (anterior-to-posterior), and FH (foot-to-head) gradients. This process culminates in 49 data points, with the initial 30 data points utilized to establish a model.

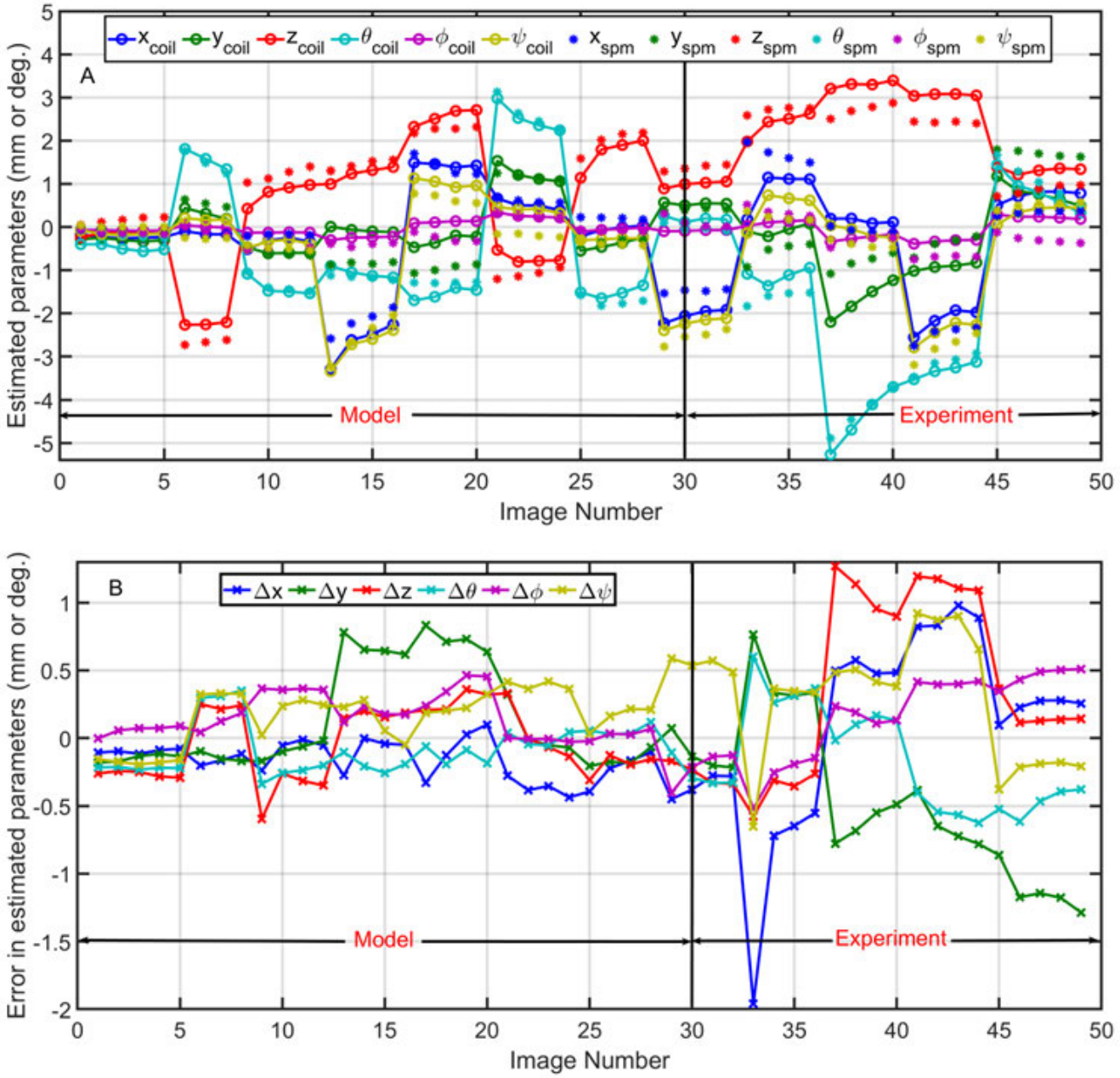

FIGURE 9. Measurements were made with short TR (TR = 2s) during scanning of the healthy subjects with a single pre-pulse applied per slice acquisition and the direction of the pre-pulse gradient cycled across volume acquisition. Change in position and orientation for subject (A). Data collection was split into a model-forming period during which positions were successively adjusted along/about a particular axis and an experimental period during which positions were randomly varied. The changes in voltages with position were characterized using data from the model-forming period. This characterization was used to estimate the position change from the voltage recordings collected during the whole experiment. The differences (×) between the position estimated with the coils (°) and using SPM8 (∗) is shown in (B) for the subject.

Using these 30 data points, a model is constructed to estimate positions for all time points. The results of this process are depicted in Figure 9. Interestingly, in this scenario, the observed error is slightly higher than what was observed with the phantom. Particularly, the maximum errors, which measure 1.2 mm, are identified along the y-translation. However, in other dimensions, the errors remain within a range of ±0.5 mm for y- and z-translations, and within ±0.5 degrees for x-, y-, and z-rotations. This outcome signifies a relatively accurate estimation, although certain translational movements exhibit more pronounced errors, especially in comparison to the less dynamic phantom-based results.

Nonetheless, this study demonstrates the feasibility of the methodology and its application in estimating positions during dynamic magnetic resonance imaging, even in the presence of motion artifacts, thereby contributing to the ongoing development of reliable imaging techniques.

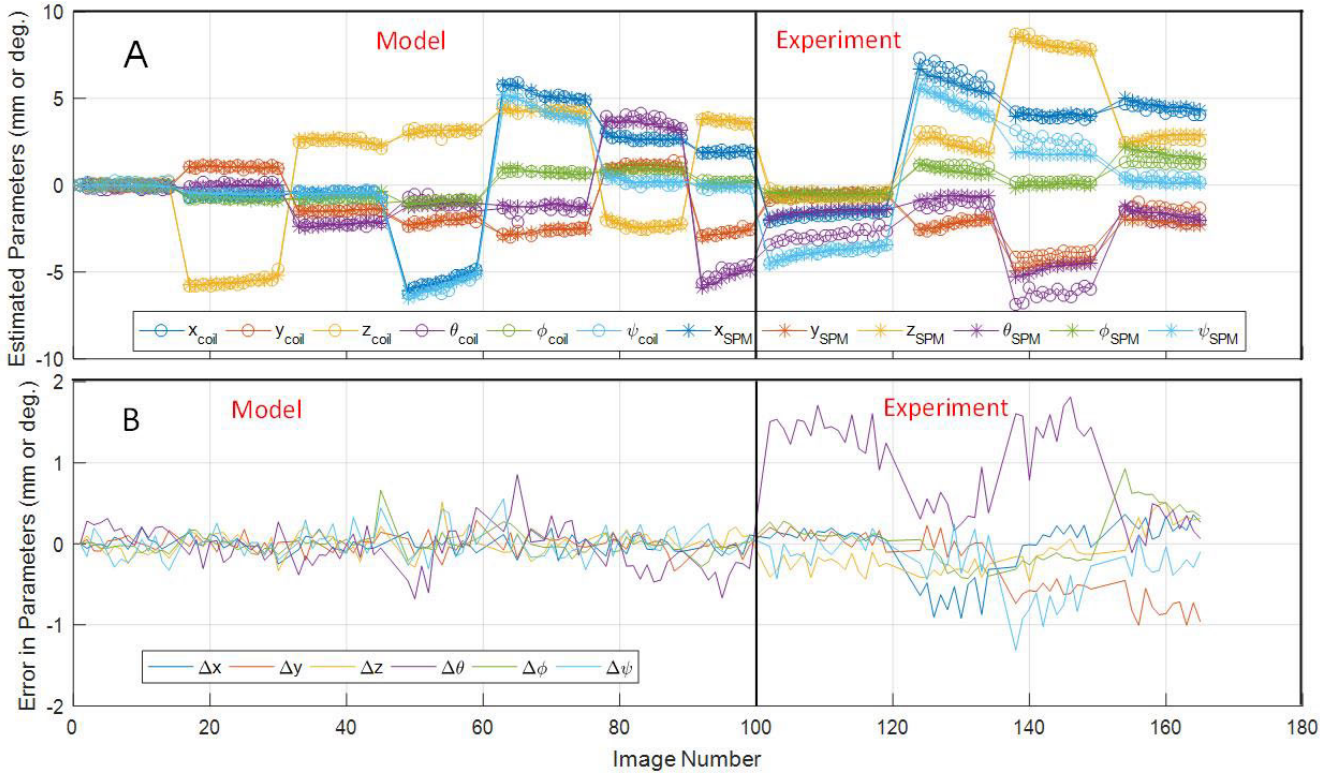

FIGURE 10. Change in position and orientation for subject (A). Measurements were made with short TR (TR = 2s) during scanning of the healthy subjects with a single pre-pulse applied per slice acquisition and the direction of the pre-pulse gradient cycled across slice acquisition. Data col- lection was split into a model-forming period during which positions were successively adjusted along/about a particular axis and an experimental period during which positions were randomly varied. The changes in voltages with position were characterized using data from the model-forming period. This characterization was used to estimate the position change from the voltage recordings collected during the whole experiment. The differences (×) between the position estimated with the coils (°) and using SPM8 (∗) is shown in (B) for the subject.

TABLE 1. Table showing the range and RMSE amplitude of the differences between the SPM8, and the induced voltage estimates of position for the phantom (calculated from 14 measurements) and the subject (determined from 5 measurements) over the experimental periods.

Error	Subject		Phantom	
	Range	RMSE	Range	RMSE
$X\ (mm)$	0.66	0.15	0.99	0.20
$Y\ (mm)$	0.54	0.15	0.53	0.14
$Z\ (mm)$	0.52	0.22	0.78	0.22
Pitch ($\theta°$)	0.66	0.21	0.73	0.20
Roll ($\varphi°$)	0.18	0.02	0.75	0.10
Yaw ($\psi°$)	0.67	0.23	0.89	0.24

Subject: Single Pre-pulses per Slice Acquisition Cycled over Slice Acquisition

To make the approach more practical, we modified the sequence so as to cycle the gradient pre-pulse axis across slice acquisitions. EPI data are again co-registered by using SPM8. We took 180 volumes and took out 15 volumes where movements occurred leaving 165 points. The first 100 volumes are used to form a model which is then applied to estimate the position during the remaining 165 volume acquisitions. The results are shown in Figure 10. Figure 10(A) shows estimated parameters by measuring the changes in induced voltage in the coils and the parameters obtained from image co-registration by using SPM8, whereas Figure 10(B) shows the difference between the two sets of parameters.

IV. DISCUSSION

Various motion tracking techniques [11], [14], [20], [21], [22], [23], [24], [25], [26], [27], [28], [29], [30], [31], [32], [33], [34], [35], [36], [37], [38], [39], [40], [41], [42], [43], [44], [45], [46], [47], [48], [49], [57], [58], [59] were introduced within the last decades. Still, there is no complete solution for involuntary head motion. Marker fixation, sequence modification, line of sight (optical tracking), artefacts (other than motion artefact) reduction is absolutely challenging. In this study, we are exploring experimental results of a model-based tracking system. The relevant theories and models are studied by Bhuiyan et al. [55].

The results of the experiments confirm that the amplitudes of the gradient-induced voltages vary linearly with changes in the coils' translational positions and with small changes in their orientations (Figure 6) and that the pattern of variation across coils is different for different types of movement (Figures 6 and 7). This allows movement information to be derived from coil measurements (Figure 7) by using a linear model incorporating coefficients calculated from a training data set for which complementary information about movement is available (e.g., from image co-registration, as used

here, or from optical or navigator-based position measurements). The results from the human subject show that this approach can provide estimates of position and orientation with less than 0.22mm and 0.24° RMS error for head movements in the range of ±4mm/degrees (Figures. 6 & 7 and in Table 1). These results were obtained by applying three pre-pulses per slice acquisition with a 400ms delay between pre-pulses, which necessitated the use of a long TR of 48s. To ensure the comfort and cooperation of the subjects, we made the decision to collect a limited number of data points. However, even with the reduced number of points, we obtained satisfactory results that met the requirements of the model.

In initial experiments, we also tested the feasibility of using short TR periods, with a single pre-pulse per volume and per slice acquisition, producing promising results as shown in Figure 8 (Phantom)-Figure 9 (Subject) and Figure 10 (subject) respectively. The relatively larger errors for the subject data compared to the phantom may be due to the use of a smaller training data set and/or the greater variety of movements in this data set during experimental period. A practical implementation of this approach would involve measuring the position-sensitive voltages induced by the imaging gradients rather than additional gradient pulses. This would speed up the model formation phase and increase the temporal resolution of position monitoring.

The maximum errors in estimated positions were not more than 1.2mm (1.2mm for y-translation, but for x- and z-translation it was less than 0.6mm or 0.6°) for the phantom, when the maximum movements were 9mm or 11° during single pre-pulse per slice acquisition cycled over volume acquisition; as shown in Figure 8. In this case, for the subject, the errors were not more than 1.9mm (1.9mm for x-translation, but for y-translation it was ∼ 1.2 and for z-translation it was less than 0.7mm or 0.6°), when the maximum movements were 4mm or 5°, as shown in Figure 9. On the other hand, the maximum errors in estimated positions were not more than 1mm or 1.8° (1.8° for x-rotation, but for x- and z-rotation it was less than 1°) for the subject when the maximum movements were 10mm or 10° during single pre-pulse per slice acquisition cycled over slice acquisition; as shown in Figure 10.

The approach used here has a few limitations. These are: image shift along the AP direction due to frequency changes, effects of vibration in the recorded voltages, effect of movement in the field and proper fixation of coils. We can overcome these by optimizing the pre-pulses, using dynamic stabilization, removing data where movement occurs and by using a tight fitting EEG-like cap. We initially reduced the effects of vibrations due to one gradient pre-pulse on the voltage measured due to later pre-pulses by using a large inter-pulse delay, which required a long TR. A more practical approach which we also tested involved using a single pre-pulse across successive acquisition.

Applying EPI with short TR produces more gradient heating which causes the passive shims to heat up, leading to a change in the B_0 field. The change in field leads to a change in resonance frequency and as a result the image shifts in the EPI phase encoding (AP) direction. The resulting image shifts along the AP direction in the absence of any kind of motion. While the measurements (model) remained unaffected by eddy currents, we will address this effect in future research.

In this paper, the results are corrected by subtracting shift in image based on prior measurements in the case of short TR both for phantom and subject. Dynamic stabilization measures the frequency in every volume acquisition and holds it constant. Dynamic stabilization will therefore help to avoid image shifts along the AP direction, but we did not used dynamic stabilization in this experiment. The strong aspect of this study is that the methods employed do not require sequence modification and can be implemented at a lower cost compared to other approaches reported in the literature.

V. CONCLUSION

We can conclude that the voltages induced in a set of coils fixed to a rigid body can be related to the position and orientation of the body. This characteristic was successfully exploited to estimate the position and orientation of an object inside the MRI scanner to within an accuracy of 0.7mm and 0.7°. While further work is required to fully optimize the approach, the principle of using a set of coils fixed to a subject's head could be used for prospective motion correction.

Further work is now needed to evaluate the efficacy of this approach for a broader range of movements of a phantom and human head. A realistic implementation of this approach would be to measure the position sensitive voltages induced by the imaging gradients of an echo-planar sequence rather than a series of additional gradient pulses. This would speed up the model formation phase, increase the temporal resolution of the position monitoring (10's of ms) and could be implemented using standard MRI sequences.

COMPETING INTERESTS

The authors declare no conflict of interests.

ACKNOWLEDGMENT

The authors would like to thank Alan Dorkes for constructing a five coils rig. The author Enamul Bhuiyan gratefully acknowledges the University of Nottingham for the Vice Chancellor Scholarship (International).

REFERENCES

[1] F. Godenschweger, U. Kägebein, D. Stucht, U. Yarach, A. Sciarra, R. Yakupov, F. Lüsebrink, P. Schulze, and O. Speck, "Motion correction in MRI of the brain," *Phys. Med. Biol.*, vol. 61, no. 5, p. R32, 2016.

[2] P. L. Young and L. A. Olsen, *The Healthcare Imperative: Lowering Costs and Improving Outcomes: Workshop Series Summary*. Washington, DC, USA: The National Academies Press, 2010, doi: 10.17226/12750.

[3] R. A. Poldrack, E. J. Paré-Blagoev, and P. E. Grant, "Pediatric functional magnetic resonance imaging: Progress and challenges," *Topics Magn. Reson. Imag.*, vol. 13, no. 1, pp. 61–70, Feb. 2002.

[4] T. T. Brown, J. M. Kuperman, M. Erhart, N. S. White, J. C. Roddey, A. Shankaranarayanan, E. T. Han, D. Rettmann, and A. M. Dale, "Prospective motion correction of high-resolution magnetic resonance imaging data in children," *NeuroImage*, vol. 53, no. 1, pp. 139–145, Oct. 2010.

[5] E. Seto, G. Sela, W. E. McIlroy, S. E. Black, W. R. Staines, M. J. Bronskill, A. R. McIntosh, and S. J. Graham, "Quantifying head motion associated with motor tasks used in fMRI," *NeuroImage*, vol. 14, no. 2, pp. 284–297, Aug. 2001.

[6] C. J. Cochrane and K. P. Ebmeier, "Diffusion tensor imaging in Parkinsonian syndromes: A systematic review and meta-analysis," *Neurology*, vol. 80, no. 9, pp. 857–864, Feb. 2013.

[7] G. T. Stebbins and C. M. Murphy, "Diffusion tensor imaging in Alzheimer's disease and mild cognitive impairment," *Behav. Neurol.*, vol. 21, no. 1, pp. 39–49, 2009.

[8] I. Bohanna, N. Georgiou-Karistianis, A. J. Hannan, and G. F. Egan, "Magnetic resonance imaging as an approach towards identifying neuropathological biomarkers for Huntington's disease," *Brain Res. Rev.*, vol. 58, no. 1, pp. 209–225, Jun. 2008.

[9] M. Inglese and M. Bester, "Diffusion imaging in multiple sclerosis: Research and clinical implications," *NMR Biomed.*, vol. 23, no. 7, pp. 865–872, Aug. 2010.

[10] J. Maclaren, M. Herbst, O. Speck, and M. Zaitsev, "Prospective motion correction in brain imaging: A review," *Magn. Reson. Med.*, vol. 69, no. 3, pp. 621–636, Mar. 2013.

[11] L. Qin, P. van Gelderen, J. A. Derbyshire, F. Jin, J. Lee, J. A. de Zwart, Y. Tao, and J. H. Duyn, "Prospective head-movement correction for high-resolution MRI using an in-bore optical tracking system," *Magn. Reson. Med.*, vol. 62, no. 4, pp. 924–934, Oct. 2009.

[12] D. MacFarlane and C. R. Wildey, "Single camera motion measurement and monitoring for magnetic resonance applications," U.S. Patent 02 30 755 A1, Sep. 22, 2011.

[13] J. Maclaren, M. Aksoy, and R. Bammer, "Contact-free physiological monitoring during simultaneous magnetic resonance imaging," U.S. Patent 03 31 239 A1, Aug. 2, 2016.

[14] T. Kober, J. P. Marques, R. Gruetter, and G. Krueger, "Head motion detection using FID navigators," *Magn. Reson. Med.*, vol. 66, no. 1, pp. 135–143, Jul. 2011.

[15] D. R. Birn, "Device for tracking head motion in an MRI simulator," Ph.D thesis, Dept. Biomed. Eng., Univ. Wisconsin-Madison, 2012.

[16] M. B. Ooi, S. Krueger, W. J. Thomas, and T. R. Brown, "Real-time intra-volume motion correction in EPI using active markers," in *Proc. 18th Annu. Meeting (ISMRM)*, 2010, p. 5038.

[17] J. Maclaren, R. Boegle, M. Herbst, J. Hennig, and M. Zaitsev, "Head pose prediction for prospectively-corrected EPI during rapid subject motion," in *Proc. 18th Annu. Meeting (ISMRM)*, 2010, p. 5031.

[18] O. Speck, J. Hennig, and M. Zaitsev, "Prospective real-time slice-by-slice motion correction for fMRI in freely moving subjects," *Magn. Reson. Mater. Phys., Biol. Med.*, vol. 19, no. 2, pp. 55–61, May 2006.

[19] R. Boegle, J. Maclaren, and M. Zaitsev, "Combining prospective motion correction and distortion correction for EPI: Towards a comprehensive correction of motion and susceptibility-induced artifacts," *Magn. Reson. Mater. Phys., Biol. Med.*, vol. 23, no. 4, pp. 263–273, Sep. 2010.

[20] H. Eviatar, J. K. Saunders, and D. I. Hoult, "Motion compensation by gradient adjustment," in *Proc. 5th Annu. Meeting (ISMRM)*, Vancouver, BC, Canada, 1997, p. 1898.

[21] H. Eviatar, B. Schattka, J. C. Sharp, J. Rendell, and M. E. Alexander, "Real time head motion correction for functional MRI," in *Proc. 7th Annu. Meeting (ISMRM)*, Philadelphia, PA, USA, 1999, p. 269.

[22] M. Herbst, J. Maclaren, J. G. Korvink, and M. Zaitsev, "A practical tracking system to avoid motion artifacts," in *Proc. 19th Annu. Meeting ISMRM*, Montreal, BC, Canada, 2011, p. 2683.

[23] M. Zaitsev, C. Dold, G. Sakas, J. Hennig, and O. Speck, "Magnetic resonance imaging of freely moving objects: Prospective real-time motion correction using an external optical motion tracking system," *NeuroImage*, vol. 31, no. 3, pp. 1038–1050, Jul. 2006.

[24] B. C. Andrews-Shigaki, B. S. R. Armstrong, M. Zaitsev, and T. Ernst, "Prospective motion correction for magnetic resonance spectroscopy using single camera retro-grate reflector optical tracking," *J. Magn. Reson. Imag.*, vol. 33, no. 2, pp. 498–504, Feb. 2011.

[25] M. Aksoy, C. Forman, M. Straka, S. Skare, S. Holdsworth, J. Hornegger, and R. Bammer, "Real-time optical motion correction for diffusion tensor imaging," *Magn. Reson. Med.*, vol. 66, no. 2, pp. 366–378, Aug. 2011.

[26] S. E. Yancey, D. J. Rotenberg, F. Tam, M. Chiew, S. Ranieri, L. Biswas, K. J. T. Anderson, S. Nicole Baker, G. A. Wright, and S. J. Graham, "Spin-history artifact during functional MRI: Potential for adaptive correction," *Med. Phys.*, vol. 38, no. 8, pp. 4634–4646, Jul. 2011.

[27] J. Schulz, T. Siegert, E. Reimer, M. Zaitsev, J. Maclaren, M. Herbst, and R. Turner, "First embedded in-bore system for fast optical prospective head motion-correction in MRI," in *Proc. 28th Annu. Sci. Meeting (ESMRMB)*, Leipzig, Germany, 2011, p. 369.

[28] J. Schulz, T. Siegert, E. Reimer, C. Labadie, J. Maclaren, M. Herbst, M. Zaitsev, and R. Turner, "An embedded optical tracking system for motion-corrected magnetic resonance imaging at 7T," *Magn. Reson. Mater. Phys., Biol. Med.*, vol. 25, no. 6, pp. 443–453, Dec. 2012.

[29] C. Forman, M. Aksoy, J. Hornegger, and R. Bammer, "Self-encoded marker for optical prospective head motion correction in MRI," *Med. Image Anal.*, vol. 15, no. 5, pp. 708–719, Oct. 2011.

[30] G. Simon, A. W. Fitzgibbon, and A. Zisserman, "Markerless tracking using planar structures in the scene," in *Proc. IEEE ACM Int. Symp. Augmented Reality (ISAR)*, Oct. 2000, pp. 120–128.

[31] J. Schaerer, A. Fassi, M. Riboldi, P. Cerveri, G. Baroni, and D. Sarrut, "Multi-dimensional respiratory motion tracking from markerless optical surface imaging based on deformable mesh registration," *Phys. Med. Biol.*, vol. 57, no. 2, pp. 357–373, Jan. 2012.

[32] C. L. Dumoulin, S. P. Souza, and R. D. Darrow, "Real-time position monitoring of invasive devices using magnetic resonance," *Magn. Reson. Med.*, vol. 29, no. 3, pp. 411–415, Mar. 1993.

[33] J. L. Ackerman, M. C. Offutt, R. B. Buxton, and T. J. Brady, "Rapid 3D tracking of small RF coils," in *Proc. 5th Annu. Meeting (ISMRM)*, Montreal, BC, Canada, 1986, pp. 1131–1132.

[34] J. A. Derbyshire, G. A. Wright, R. M. Henkelman, and R. S. Hinks, "Dynamic scan-plane tracking using MR position monitoring," *J. Magn. Reson. Imag.*, vol. 8, no. 4, pp. 924–932, Jul. 1998.

[35] M. B. Ooi, S. Krueger, W. J. Thomas, S. V. Swaminathan, and T. R. Brown, "Prospective real-time correction for arbitrary head motion using active markers," *Magn. Reson. Med.*, vol. 62, no. 4, pp. 943–954, Oct. 2009.

[36] M. B. Ooi, S. Krueger, J. Muraskin, W. J. Thomas, and T. R. Brown, "Echo-planar imaging with prospective slice-by-slice motion correction using active markers," *Magn. Reson. Med.*, vol. 66, no. 1, pp. 73–81, Jul. 2011.

[37] C. Barmet, N. D. Zanche, and K. P. Pruessmann, "Spatiotemporal magnetic field monitoring for MR," *Magn. Reson. Med.*, vol. 60, no. 1, pp. 187–197, Jul. 2008.

[38] C. Barmet, N. De Zanche, B. J. Wilm, and K. P. Pruessmann, "A transmit/receive system for magnetic field monitoring of in vivo MRI," *Magn. Reson. Med.*, vol. 62, no. 1, pp. 269–276, Jul. 2009.

[39] M. B. Ooi, M. Aksoy, J. Maclaren, R. D. Watkins, and R. Bammer, "Prospective motion correction using inductively coupled wireless RF coils," *Magn. Reson. Med.*, vol. 70, no. 3, pp. 639–647, Sep. 2013.

[40] L. Qin, E. J. Schmidt, Z. T. H. Tse, J. Santos, W. S. Hoge, C. Tempany-Afdhal, K. Butts-Pauly, and C. L. Dumoulin, "Prospective motion correction using tracking coils," *Magn. Reson. Med.*, vol. 69, no. 3, pp. 749–759, Mar. 2013.

[41] A. J. W. van der Kouwe, T. Benner, and A. M. Dale, "Real-time rigid body motion correction and shimming using cloverleaf navigators," *Magn. Reson. Med.*, vol. 56, no. 5, pp. 1019–1032, Nov. 2006.

[42] H. A. Ward, S. J. Riederer, R. C. Grimm, R. L. Ehman, J. P. Felmlee, and C. R. Jack, "Prospective multiaxial motion correction for fMRI," *Magn. Reson. Med.*, vol. 43, no. 3, pp. 459–469, Mar. 2000.

[43] E. B. Welch, A. Manduca, R. C. Grimm, H. A. Ward, and C. R. Jack, "Spherical navigator echoes for full 3D rigid body motion measurement in MRI," *Magn. Reson. Med.*, vol. 47, no. 1, pp. 32–41, Jan. 2002.

[44] N. White, C. Roddey, A. Shankaranarayanan, E. Han, D. Rettmann, J. Santos, J. Kuperman, and A. Dale, "PROMO: Real-time prospective motion correction in MRI using image-based tracking," *Magn. Reson. Med.*, vol. 63, no. 1, pp. 91–105, Jan. 2010.

[45] M. D. Tisdall, A. T. Hess, M. Reuter, E. M. Meintjes, B. Fischl, and A. J. W. van der Kouwe, "Volumetric navigators for prospective motion correction and selective reacquisition in neuroanatomical MRI," *Magn. Reson. Med.*, vol. 68, no. 2, pp. 389–399, Aug. 2012.

[46] A. Alhamud, M. D. Tisdall, A. T. Hess, K. M. Hasan, E. M. Meintjes, and A. J. W. van der Kouwe, "Volumetric navigators for real-time motion correction in diffusion tensor imaging," *Magn. Reson. Med.*, vol. 68, no. 4, pp. 1097–1108, Oct. 2012.

[47] D. S. Illera, D. C. Nollb, and J. A. Fesslera, "Prospective motion correction for functional MRI using sparsity and Kalman filtering," *Proc. SPIE*, vol. 8858, Sep. 2013, Art. no. 885823.

[48] J. G. Pipe, "Motion correction with PROPELLER MRI: Application to head motion and free-breathing cardiac imaging," *Magn. Reson. Med.*, vol. 42, no. 5, pp. 963–969, Nov. 1999.

[49] M. Andersen, K. H. Madsen, and L. G. Hanson, "Prospective motion correction for MRI using EEG-equipment," in *Proc. 24th Annu. Meeting Exhib.*, 2016, p. 4254.
[50] P. R. Jensen, C. Benjaminsen, A. E. Hansen, R. Larsen, and O. V. Olesen, "Markerless motion correction in MRI," in *Proc. ISMRM*, 2015, p. 587.
[51] M. B. Vestergaard, J. Schulz, R. Turner, and L. G. Hanson, "Motion tracking from gradient induced signals in electrode recordings," in *Proc. Congr. ESMRMB*, 2011, p. 368.
[52] E. H. Bhuiyan, M. E. H. Chowdhury, P. M. Glover, and R. Bowtell, "Movement monitoring for MRI via measurement of changes in the gradient induced EMF in coil arrays," in *Proc. Int. Soc. Mag. Reson. Med.*, vol. 23, 2015, p. 1017.
[53] J. L. Crowley, F. Wallner, and B. Schiele, "Position estimation using principal components of range data," *Robot. Auto. Syst.*, vol. 23, no. 4, pp. 267–276, Jul. 1998.
[54] B. D. D. Senneville, A. El Hamidi, and C. Moonen, "A direct PCA-based approach for real-time description of physiological organ deformations," *IEEE Trans. Med. Imag.*, vol. 34, no. 4, pp. 974–982, Apr. 2015.
[55] E. H. Bhuiyan, M. E. H. Chowdhury, and P. M. Glover, "Feasibility of tracking involuntary head movement for MRI using a coil as a magnetic dipole in a time-varying gradient," *Magn. Reson. Imag.*, vol. 101, pp. 76–89, Sep. 2023.
[56] A. Roth and E. Nevo, "Method and apparatus to estimate location and orientation of objects during magnetic resonance imaging," U.S. Patent 9 037 213, May 19, 2015.
[57] R. Frost, P. Wighton, F. I. Karahanoğlu, R. L. Robertson, P. E. Grant, B. Fischl, M. D. Tisdall, and A. van der Kouwe, "Markerless high-frequency prospective motion correction for neuroanatomical MRI," *Magn. Reson. Med.*, vol. 82, no. 1, pp. 126–144, Jul. 2019.
[58] M. Laustsen, M. Andersen, R. Xue, K. H. Madsen, and L. G. Hanson, "Tracking of rigid head motion during MRI using an EEG system," *Magn. Reson. Med.*, vol. 88, no. 2, pp. 986–1001, 2022.
[59] O. Afacan, T. E. Wallace, and S. K. Warfield, "Retrospective correction of head motion using measurements from an electromagnetic tracker," *Magn. Reson. Med.*, vol. 83, no. 2, pp. 427–437, Feb. 2020.
[60] M. Haeberlin, L. Kasper, C. Barmet, D. O. Brunner, B. E. Dietrich, S. Gross, B. J. Wilm, S. Kozerke, and K. P. Pruessmann, "Real-time motion correction using gradient tones and head-mounted NMR field probes," *Magn. Reson. Med.*, vol. 74, no. 3, pp. 647–660, Sep. 2015.
[61] J. Levitt, A. van der Kouwe, H. Jeong, L. D. Lewis, and G. Bonmassar, "The MotoNet: A 3 Tesla MRI-conditional EEG net with embedded motion sensors," *Sensors*, vol. 23, no. 7, p. 3539, Mar. 2023.
[62] O. V. Olesen, R. R. Paulsen, L. Hojgaard, B. Roed, and R. Larsen, "Motion tracking for medical imaging: A nonvisible structured light tracking approach," *IEEE Trans. Med. Imag.*, vol. 31, no. 1, pp. 79–87, Jan. 2012.
[63] M. E. H. Chowdhury, K. J. Mullinger, P. Glover, and R. Bowtell, "Reference layer artefact subtraction (RLAS): A novel method of minimizing EEG artefacts during simultaneous fMRI," *NeuroImage*, vol. 84, pp. 307–319, Jan. 2014.

ENAMUL H. BHUIYAN received the B.Sc. degree in physics from the University of Dhaka, the M.Sc. degree in physics from Laurentian University, Canada, and the Ph.D. degree in physics from the University of Nottingham, U.K. He was a Postdoctoral Fellow with the Department of Radiology, The Biomedical Engineering and Imaging Institute, Icahn School of Medicine at Mount Sinai, where he focused on developing methods for body imaging, such as DCE-MRI, DWI, and motion-robust liver imaging, with an emphasis on liver cancer, particularly hepatocellular carcinoma (HCC). Previously, he was a Postdoctoral Associate with the Department of Radiology and Biomedical Imaging, Yale School of Medicine. During this time, he was involved in developing new methods in MRI and MR pulse sequences, including image encoding with nonlinear gradients and novel contrast mechanisms, as well as various methods of image reconstruction. He is currently a Research Scientist with the Center for Magnetic Resonance Research, University of Illinois at Chicago. He conducted research on DWI for diagnosing prostate cancer. His research interests include developing new hardware and software methods for biomedical imaging using physics and mathematics and utilizing modern image reconstruction techniques and image analysis to understand brain physiology and functions. He is also interested in using these methods as biomarkers for neurological diseases and disorders.

MUHAMMAD E. H. CHOWDHURY (Senior Member, IEEE) received the Ph.D. degree from the University of Nottingham, Nottingham, U.K., in 2014. He was a Postdoctoral Research Fellow with the Sir Peter Mansfield Imaging Centre, University of Nottingham. He is currently an Assistant Professor with the Department of Electrical Engineering, Qatar University. He is running NPRP, UREP, and HSREP grants from the Qatar National Research Fund (QNRF) and internal grants (IRCC and HIG) from Qatar University along with academic projects from HBKU and HMC. He has filed several patents and published more than 140 peer-reviewed journal articles, more than 30 conference papers, and several book chapters. His current research interests include biomedical instrumentation, signal processing, wearable sensors, medical image analysis, machine learning and computer vision, embedded system design, and simultaneous EEG/fMRI. He is a member of the British Radiology, ISMRM, and HBM. He has recently won the COVID-19 Dataset Award, the AHS Award from HMC, and the National AI Competition awards for the contribution to the fight against COVID-19. His team is the gold medalist at the 13th International Invention Fair in the Middle East (IIFME). He is serving as the Guest Editor for *Polymers*, an Associate Editor for IEEE Access, and a Topic Editor and Review Editor for *Frontiers in Neuroscience*. He has been listed among the Top 2% of scientists in the World List–2022, published by Stanford University.

PAUL M. GLOVER was born in Derby. He received the Ph.D. degree in electronic engineering from Hull University, in 1982. He started the career with the Sir Peter Mansfield Imaging Centre, University of Nottingham, in magnetic resonance imaging scanners, where he became a Lecturer. Previously, he was with the University of Surrey, and then back with the University of Nottingham. He continues the research ways of making MRI faster, better, and quieter, which in turn allows MRI to make better clinical diagnosis and treatment possible. Most recently, he has become intrigued by the safety aspects of MRI and the effects of magnetic fields on the human body, particularly why people feel dizzy in very strong magnetic fields. His current research interests include developments and applications of magnetic resonance imaging and the design of radio-frequency probes to generate the required excitation fields and to pick up the signals. At high frequencies, the short wavelength causes problems with image homogeneity. By careful design and using new multiple transmit methods, these problems can be overcome. He is also researching the use of high-temperature superconductive probes in MRI. His other area of interest is that of the safety of magnetic fields and their interaction with the human body. Working in and around very high magnetic fields can cause dizziness, a metallic taste in the mouth, and flashing lights in the eyes. Understanding the interaction mechanisms fully should lead to appropriate safety legislation related to magnetic fields.